GEOPHYSICS, VOL. 72, NO. 1 (JANUARY-FEBRUARY 2007); P. V21–V32, 12 FIGS., 1 TABLE.
10.1190/1.2399442

Fourier reconstruction of nonuniformly sampled, aliased seismic data

P. M. Zwartjes[1] and M. D. Sacchi[2]

ABSTRACT

There are numerous methods for interpolating uniformly sampled, aliased seismic data, but few can handle the combination of nonuniform sampling and aliasing. We combine the principles of Fourier reconstruction of nonaliased, nonuniformly sampled data with the ideas of frequency-wavenumber (f-k) interpolation of aliased, uniformly sampled data in a new two-step algorithm. In the first step, we estimate the Fourier coefficients at the lower nonaliased temporal frequencies from the nonuniformly sampled data. The coefficients are then used in the second step as an a priori model to distinguish between aliased and nonaliased energy at the higher, aliased temporal frequencies. By using a nonquadratic model penalty in the inversion, both the artifacts in the Fourier domain from nonuniform sampling and the aliased energy are suppressed. The underlying assumption is that events are planar; therefore, the algorithm is applied to seismic data in overlapping spatiotemporal windows.

INTRODUCTION

In seismic data acquisition the spatial sampling is such that aliasing occurs often. Interpolation of uniformly sampled, nonaliased seismic data is straightforward and can be performed by convolution with a sinc filter in the spatial domain or by extending the Nyquist wavenumber of a band-limited signal through zero padding in the Fourier domain. If aliasing on seismic shot records can be removed by reducing the spatial bandwidth with NMO, such simple interpolation methods are sufficient for interpolation. However, coherent noise such as multiples and groundroll may still be aliased after NMO.

Interpolation of spatially aliased data is less trivial, but a variety of methods has been published in the geophysical literature; see Gulunay (2003) for an overview. Methods based on the dip scan or slant-stack approach scan along a limited number of dips in a small window to identify the main events, which are then interpolated along the identified dip to a finer grid [see, for instance, Bardan (1987); Kao (1997)]. The frequency-space (f-x) interpolation method by Spitz (1991) uses the predictability of stationary, nondispersive, planar events to interpolate aliased data at high temporal frequencies with filters derived at the nonaliased lower frequencies. Closely related is the method of f-x projection filters, which differs in the definition of the noise model (Soubaras, 1997). The time-space (t-x) domain interpolation by Claerbout and Nichols (1991) also falls into the category of filter-based interpolation techniques and uses 2D prediction filters in the time-space domain to predict traces at a smaller sampling interval. Crawely and Clapp (1999) extend the t-x domain prediction-error filtering approach to handle nonstationary events.

More recently, Fomel (2002) has presented a t-x domain interpolation technique based on plane-wave destruction filters that is an alternative to the t-x and f-x prediction filter approaches. Among the benefits of this method are (1) it handles nonstationary events and (2) the obtained coefficients are interpreted as local slope, which has a range of applications. If convolution of aliased data along the spatial axis with an appropriate filter yields nonaliased data, then the same result can be achieved in the wavenumber domain by multiplication of the aliased spectra with an appropriate mask. This is the approach of Gulunay (2003), who also uses the nonaliased lower frequencies to attack the aliases. In fact, the methods of Spitz and Gulunay are equivalent but are implemented in different domains (Gulunay, 2003). The use of nonaliased lower temporal frequencies to dealias higher frequencies has also been applied successfully by Herrmann et al. (2000) for the high-resolution Radon transform.

Abma and Kabir (2003) compare various t-x, f-x, and frequency-wavenumber (f-k) methods qualitatively and conclude that there are some differences in speed and reconstruction quality, depending on the trace density and complexity of the input data. The following assumptions are common to these methods. First, the data are assumed to consist of planar events. If this is not the case, the method must be applied in small spatiotemporal windows in which the assumption of

Manuscript received by the Editor August 6, 2005; revised manuscript received July 13, 2006; published online December 29, 2006.
[1]Formerly Delft University of Technology; presently Shell International Exploration and Production, Kessler Park 1, 2288 GS Rijswijk, the Netherlands. E-mail: paul.zwartjes@shell.com.
[2]University of Alberta, Department of Physics, Edmonton, Alberta T6G 2J1, Canada. E-mail: sacchi@phys.ualberta.ca.

planar events approximately holds. Second, the range of dips in the data is limited. Third, if the data consist of planar events, the lower temporal frequencies in the *f-k* spectrum are nonaliased and can be used to distinguish aliased from nonaliased energy at higher temporal frequencies. Fourth, the data are sampled uniformly. The last assumption of uniform sampling is a requirement for the *f-k* and *t-x*, *f-x* prediction filter algorithms. It is not a requirement for the slant-stack/dip-scan methods Kao (1997).

Of the numerous methods for interpolating aliased seismic data, very few can handle nonuniform sampling. The objective of this paper, therefore, is to propose a method that can interpolate aliased seismic data and is robust against sampling irregularities. We combine the principles of Fourier reconstruction of nonaliased, nonuniformly sampled data, which can handle nonuniform sampling, with the ideas of Gulunay's *f-k* interpolation of aliased uniformly sampled data in a new two-stage algorithm. In the first step of this algorithm, only the Fourier coefficients of the nonaliased, lower temporal frequencies are estimated. These are then used to construct a matrix with model weighting terms, similar to the principles of Gulunay's *f-k*-domain mask that suppress aliasing. This matrix is used in the second step to discriminate between aliased and nonaliased energy in the entire spectrum. By using a nonquadratic model penalty in the inversion, both Fourier domain artifacts from nonuniform sampling and aliased energy are suppressed.

The underlying assumption is that events are planar; therefore, the algorithm is applied to seismic data in overlapping spatiotemporal windows. The maximum temporal frequency that can be corrected for aliasing depends on the highest nonaliased temporal frequency. As the aliasing becomes more severe, the nonaliased region shrinks. So there is a limit to how much aliasing can be handled. Additionally, the algorithm only discriminates between aliased and nonaliased coefficients and cannot discriminate between aliased and nonaliased energy for a single coefficient. For this reason, overlapping of aliased and nonaliased energy still presents a challenge. As the sampling becomes more nonuniform, the spectrum becomes more distorted to the point where aliasing is no longer an issue. Therefore, for randomly sampled data, both the new two-stage algorithm and the standard Fourier reconstruction yield equally good results. For uniformly sampled and moderately nonuniformly sampled data, good results have been obtained on 1D field data and on 1D and 2D synthetic data.

Fourier reconstruction of nonuniformly sampled, aliased seismic data

Fourier reconstruction Duijndam et al. (1999) is a method to interpolate nonuniformly sampled data, which can be uniform sampling with missing traces, uniform sampling with random deviations, or fully random sampling. It assumes band-limited data and therefore is unsuited for aliased data. In this article, we discuss how Fourier reconstruction can be used on nonuniformly sampled, aliased data using the assumptions mentioned in the previous paragraph. With respect to these assumptions, the following comments apply. We assume the data to consist of a limited number of planar events, a valid assumption when the algorithm is applied in small windows. We use the nonaliased part of the spectrum to generate model weights for the inversion in Fourier reconstruction, and we use these weights to suppress aliased energy. The generation of the weights is inspired by the *f-k* interpolation method for aliased data Gulunay (2003). We do not assume uniform sampling because nonuniform sampling artifacts are taken care of by Fourier reconstruction. We first discuss nonuniform sampling and its effect on the discrete Fourier transform (DFT).

Nonuniform discrete Fourier transform

When data $p[x_n]$ are nonuniformly sampled at locations $[x_0, \ldots, x_{N-1}]$, we can use the nonuniform discrete Fourier transform (NDFT) to compute the Fourier coefficients:

$$\tilde{p}_{\mathrm{NDFT}}[m\Delta k] = \sum_{n=0}^{N-1} p[x_n] e^{jm\Delta k x_n} \Delta x_n. \tag{1}$$

Trace weights are used to compensate for differences in sampling density and are scaled such that $\Sigma_n \Delta x_n = \Delta k/2\pi$. The spatial bandwidth is $[-M\Delta k/2, \ldots, M\Delta k/2 - 1]$ with $\Delta k = 2\pi/(x_{N-1} - x_0)$. Now assume we have obtained discrete Fourier coefficients from data sampled on a regular grid in the spatial domain. These coefficients are denoted by $\tilde{\mathbf{p}}_{\mathrm{DFT}}$. The inverse transform from a uniformly sampled *k*-space $\tilde{\mathbf{p}}_{\mathrm{DFT}}$ to a nonuniformly sampled spatial grid is

$$p[x_n] = \frac{\Delta k}{2\pi} \sum_{m=-M/2}^{M/2-1} \tilde{p}_{\mathrm{DFT}}[m\Delta k] e^{-jm\Delta k x_n}. \tag{2}$$

Duijndam and Schonewille (1999) present a fast algorithm to compute the NDFT. The NDFT coefficients equal the DFT coefficients convolved with the NDFT of the sampling weights. This follows from substituting of equation 2, the inverse NDFT, in equation 1, the forward DFT:

$$\begin{aligned}\tilde{p}_{\mathrm{NDFT}}[m\Delta k] &= \frac{\Delta k}{2\pi} \sum_n \sum_q \tilde{p}_{\mathrm{DFT}}[q\Delta k] e^{-jq\Delta k x_n} e^{jm\Delta k x_n} \Delta x_n \\ &= \frac{\Delta k}{2\pi} \sum_q \sum_n \Delta x_n e^{j(m-q)\Delta k x_n} \tilde{p}_{\mathrm{DFT}}[q\Delta k] \qquad (3) \\ &= \{\mathrm{PSF} * \tilde{p}_{\mathrm{DFT}}\}[m\Delta k]. \qquad (4)\end{aligned}$$

In equation 4, PSF stands for *point-spread function* and is defined as the NDFT of the trace weights:

$$\mathrm{PSF}[m\Delta k] = \frac{\Delta k}{2\pi} \sum_{n=0}^{N-1} \Delta x_n e^{jm\Delta k x_n}. \tag{5}$$

The distortion in the NDFT is determined by the PSF, which in turn is influenced by the weights. As the PSF approaches a delta function, the NDFT becomes more like the DFT.

Sampling-related problems: Aliasing and sampling artifacts

Sampling involves multiplying a continuous signal with a discrete sampling train *s* (Figure 1a). The analog in the Fourier domain is to convolve the signal spectrum with the Fourier transform of *s*, i.e., $\tilde{s}$ (Figure 1b), which yields an infinite number of aliases of the original

spectrum. The periodicity of the aliases in the Fourier domain is determined by the spatial sampling interval. If the bandwidth of the signal exceeds the periodicity of $\tilde{s}$, then spatial aliasing occurs, as shown on the planar events in Figure 2a and b.

In the case of uniform sampling with missing samples, aliases still occur in the Fourier domain, but now the periodicity is determined by the smallest sampling interval (Figure 1c–f). Random sampling can be thought of as uniform sampling with missing samples on a very finely sampled underlying grid. The aliases in the Fourier domain are then so widely spaced that the aliasing effect is effectively absent (Figure 1g–j).

Another effect of nonuniform sampling is that $\tilde{s}$ is no longer a perfect spike train but contains artifacts between its spikes. These artifacts indicate how much a single Fourier coefficient is distorted by the PSF in equation 5. Convolution with this noisy spike train distorts the Fourier coefficients. Figure 1c and 1e shows the case of uniform sampling where positions have been omitted such that, respectively, 50 and 15 samples remain. Note the PSF and the periodicity in $\tilde{s}$ (Figure 1d and f). Figure 1g–j shows s and $\tilde{s}$ for random sampling with 50 and 15 positions, respectively. Here, the spike series that causes the aliases of the spectrum is absent.

Figure 2 shows the effect of spatial sampling on the estimate of the spectrum for cross-dipping, aliased linear events. Figure 2a shows the case of uniform samping; its spectrum in Figure 2b is aliased but without artifacts. When the sampling is uniform with gaps caused by missing traces (Figure 2c), the spectrum again shows aliasing but now also artifacts from sampling irregularities. This is explained by the convolution of the true spectrum with a noisy spike train such as in Figure 1d. In the case of random sampling (Figure 2e), the artifacts in the spectrum are still there; but because of the absence of replicating spikes (see, for instance, Figure 1h), the spectrum is not aliased.

In practice, sampling is not always uniform with missing samples nor fully random. Starting from uniform sampling with or without missing positions, the sampling locations can be perturbed more and more to yield increasingly nonuniform sampling patterns. As sampling of seismic data becomes more nonuniform, the aliasing becomes more and more diffuse until it disappears altogether for random sampling.

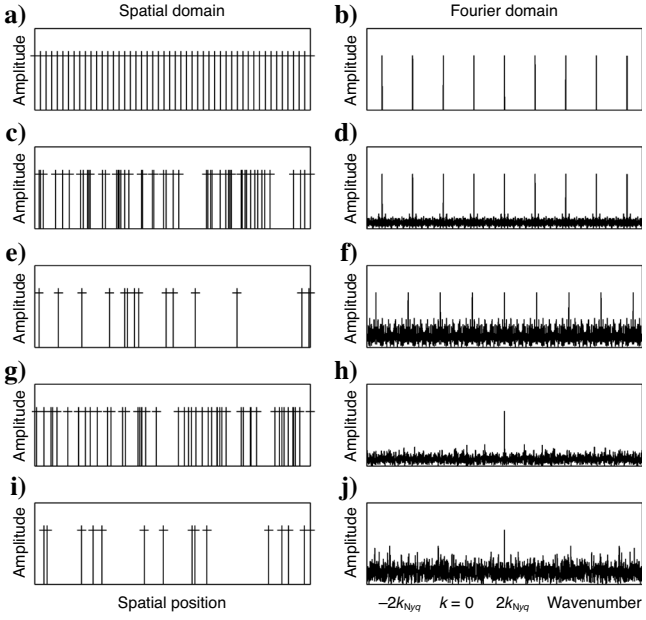

Figure 1. A schematic sampling train in the spatial domain. (a) Uniform sampling. (c) and (e) Nonuniform sampling with 50 and 15 positions. (g) and (i) Random sampling with 50 and 15 positions. The figures in the right column (b), (d), (f), (h), and (j) show the spectra of the figures in the left column, obtained using NDFT (equation 1). The central spike denotes $k = 0$, and all other spikes are its replications that are the cause of aliasing. Note the lack of these replications for random sampling in (h) and (j).

FOURIER RECONSTRUCTION WITH SPARSE INVERSION (FRSI)

The NDFT coefficients equal the DFT coefficients convolved with the PSF of the nonuniform grid. A reconstruction procedure that contains a deconvolution for the PSF is therefore a logical approach to the problem (Feichtinger et al., 1995; Duijndam et al., 1999). This is done with least-squares inversion per temporal frequency ω as Fourier reconstruction is applied to the nonuniformly sampled spatial coordinates. Inversion requires a forward-modeling step, and for

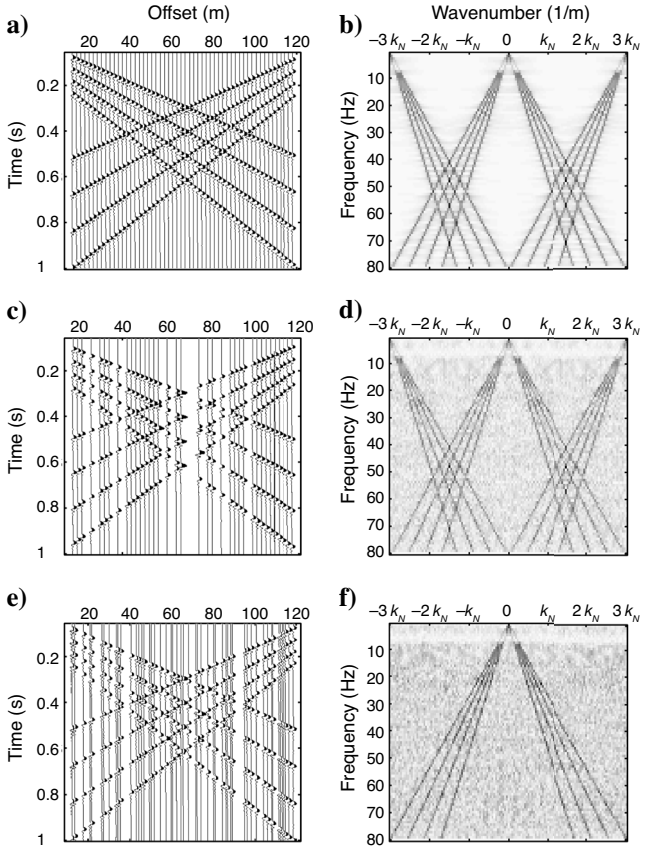

Figure 2. Linear events sampled (a) uniformly, (c) uniformly with missing traces and (e) randomly. (b), (d), and (f) Corresponding spectra computed with NDFT (k_N denotes Nyquist).

Fourier reconstruction, this is equation 2, the inverse DFT to a nonuniform grid. Instead of a quadratic penalty function that minimizes the model norm and yields a smooth model, one could look for a parsimonious model structure or sparse solution. Such models can be obtained with nonquadratic regularization terms that penalize smooth and favor sparse models. In robust regression, nonquadratic penalties are imposed on the residual. In sparse inversion, they are imposed on the model parameters. The damping factor that results from a quadratic model penalty function penalizes all model parameters. A nonquadratic model penalty function penalizes (or weighs) the large model parameters less than the smaller ones. Parameters that receive more weight are damped more, and in this manner the model penalty enforces sparseness in the model. This approach of Fourier reconstruction with sparse inversion (FRSI) improves the reconstruction result, as shown by Sacchi and Ulrych (1996), Zwartjes and Duijndam (2000), and Liu and Sacchi (2001). The effect of the nonquadratic constraint is to suppress sampling and aperture-related artifacts, which has also been used to great advantage in the high-resolution Radon transform (Sacchi and Ulrych, 1995; Trad et al., 2003).

One of the earliest applications of nonquadratic penalties in the field of geophysics was for robust regression (Claerbout and Muir, 1973). Thorson and Claerbout (1985) use a mix of quadratic model penalties to obtain a sparse hyperbolic Radon transform, and Sacchi and Ulrych (1995) obtain similar results using a single nonquadratic penalty in their high-resolution parabolic Radon transform. Other applications are in crosshole tomography (Clippard et al., 1995), in 3D multiple prediction (van Dedem and Verschuur, 2000), and in least-squares migration (Liu et al., 2003). The application of nonquadratic model penalties for seismic data regularization with the Fourier transform started with Sacchi and Ulrych (1996) and was extended by Zwartjes and Hindriks (2001) for sampling problems in two spatial dimensions and by Liu (2004) for four spatial dimensions. Similar algorithms have been presented by Wajer et al. (1998) in the field of magnetic resonance imaging (MRI) for reconstructing nonuniformly sampled Fourier space data.

Xu et al. (2005) discuss an alternative algorithm that uses only the NDFT for reconstruction and can be applied to nonuniformly sampled data. In each iteration of the algorithm, only the largest NDFT coefficient is inverse Fourier transformed to the original nonuniform grid and subtracted from the data. This is repeated until there is no signal left or until a user-specified threshold is reached. The coefficients retrieved at each iteration are stored, and from these the signal is reconstructed on a uniformly spaced grid. This is very similar to the so-called CLEAN algorithm by (Högbom, 1974), but that contains a least-squares fit for each retrieved coefficient, whereas Xu et al. (2005) only uses the NDFT. The result of that method therefore depends on the quality of the NDFT, which deteriorates as the sampling becomes less uniform. Because of the repeated evaluation of the forward and inverse NDFT, both algorithms can be quite slow for random sampling grids, although on uniformly spaced grids with missing samples the FFT can be used. Xu et al. (2005) claim the method also works in the presence of aliasing, although no details are given in the paper.

The goal in Fourier reconstruction with sparse inversion is to minimize the following objective function:

$$J = \frac{1}{\sigma_n^2}\|\mathbf{W}^{1/2}(\mathbf{p} - \mathbf{A}\tilde{\mathbf{p}})\|_2^2 + \rho(\tilde{\mathbf{p}}). \tag{6}$$

The first term on the right side of equation 6 is the data-fit term, and the second term is the model penalty term. The symbols are defined as

$$p_n = p[x_n],$$

$$A_{nm} = \frac{\Delta k}{2\pi} e^{-jm\Delta k x_n},$$

$$\tilde{p}_m = \tilde{p}_{\mathrm{DFT}}[m\Delta k].$$

$$W_{nn} = \Delta x_n,$$

$$\rho(\tilde{p}_m) = \frac{1}{2(1-a)}(\tilde{p}_m^2 + 1)^{1-a}.$$

The term σ_n^2 is noise variance, and $\mathbf{p}$ and $\tilde{\mathbf{p}}$ are vectors. For reconstruction in one spatial dimension, a simple weighting scheme, such as

$$\Delta x_n = \frac{1}{2}(x_{n+1} - x_{n-1}), \tag{7}$$

increases the convergence of the conjugate gradient scheme (Feichtinger et al., 1995). In two spatial dimensions, the choice of a trace weighting scheme is less straightforward. One approach is to use weights proportional to the area surrounding the nth trace, as determined by Voronoi cells (Hindriks and Duijndam, 2000). This approach to construction of weights is driven by considerations in the spatial domain. Pipe and Menon (1999) present an alternative approach for constructing weights for sampling problems in the field of MRI. Their method iteratively adjusts the weights such that the PSF defined in equation 5 approaches a 2D delta function. Both approaches can be extended to higher spatial dimensions, although in the presence of large gaps, one should be careful of assigning large weights to bad traces.

The minimum of the objective function in equation 6 is given by

$$\hat{\tilde{\mathbf{p}}} = (\mathbf{A}^H\mathbf{W}\mathbf{A} + \sigma_n^2\mathbf{C}_{\tilde{p}})^{-1}\mathbf{A}^H\mathbf{W}\mathbf{p}, \tag{8}$$

with

$$[\mathbf{C}_{\tilde{p}}]_{mm} = (\sigma_p^2 + \tilde{p}_i^*\tilde{p}_i)^a. \tag{9}$$

The scalars σ_n^2 and $\sigma_{\tilde{p}}^2$ are related to the noise and signal variances, whereas a describes the model parameter distribution. In practice, these parameters are used as inversion tuning parameters. Including the nonquadratic model penalty term in the objective function yields a sparse inversion estimator. Any nonquadratic penalty function that has been successfully used for robust regression of noisy data can be used for sparse inversion. However, no penalty function is best for all applications, and many different nonquadratic penalty functions have appeared and will probably continue to appear in the literature. Because of the ambiguity in choosing a model penalty function, we use a new weighting function, defined in equation 9, which allow us to tune the amount of sparseness through the scale parameters a and $\sigma_{\tilde{p}}^2$. For $a = 1/2$, this corresponds to the derivative with respect to $\tilde{p}$

of the convex ℓ_{1-2} function (a smooth approximation to the discontinuous ℓ_1-norm). For $a = 1$ and $a = 2$, it corresponds to the nonconvex Cauchy and Geman-McClure penalty functions, respectively. See Zhang (1997) for a description of these and other penalty functions. The matrix $\mathbf{C}_{\tilde{p}}$ can be interpreted as the model covariance matrix, with variances defined by equation 9, the model weighting function.

The inversion for the Fourier coefficients can be performed with an efficient conjugate gradient scheme that takes advantage of the Toeplitz matrix in the normal equations. Preconditioning is used to reduce the number of iterations required for convergence and, hence, to speed the inversion. Like many authors before us (Hansen, 1998; Trad et al., 2003; Claerbout and Fomel, 2004 and references), we bring the linear system to standard form. This is equivalent to using a preconditioned conjugate gradient scheme with the weight matrix $\mathbf{C}_{\tilde{p}}$ as a preconditioner.

The objective function of penalized likelihood estimation,

$$J = \frac{1}{\sigma_n^2}\|\mathbf{W}^{1/2}(\mathbf{p} - \mathbf{A}\tilde{\mathbf{p}})\|_2^2 + \|\mathbf{C}_{\tilde{p}}^{-1/2}\tilde{\mathbf{p}}\|_2^2, \quad (10)$$

is brought to standard form by a coordinate transformation $\mathbf{z} = \mathbf{C}_{\tilde{p}}^{-1/2}\tilde{\mathbf{p}}$,

$$J = \frac{1}{\sigma_n^2}\|\mathbf{W}^{1/2}(\mathbf{p} - \mathbf{A}'\mathbf{z})\|_2^2 + \|\mathbf{z}\|_2^2, \quad (11)$$

where $\mathbf{A}' = \mathbf{A}\mathbf{C}_{\tilde{p}}^{1/2}$. The estimator obtained by minimizing equation 11 is

$$\tilde{\mathbf{z}} = (\mathbf{A}'^H\mathbf{W}\mathbf{A}' + \sigma_n^2\mathbf{I})^{-1}\mathbf{A}'^H\mathbf{W}\mathbf{p}, \quad (12)$$

or, in terms of the original model,

$$\hat{\tilde{\mathbf{p}}} = \mathbf{C}_{\tilde{p}}^{1/2}(\mathbf{C}_{\tilde{p}}^{1/2}\mathbf{A}^H\mathbf{W}\mathbf{A}\mathbf{C}_{\tilde{p}}^{1/2} + \sigma_n^2\mathbf{I})^{-1}\mathbf{C}_{\tilde{p}}^{1/2}\mathbf{A}^H\mathbf{W}\mathbf{p}. \quad (13)$$

IRLS with preconditioned conjugate gradient for normal equations (CGNE)

We solve equation 13 via iteratively reweighted least squares (IRLS), i.e., repeated application of the CGNE scheme to the linearized problem, updating the nonlinear term after each IRLS iteration. Claerbout and Fomel (2004) discuss preconditioned inversion in interpolation with prediction-error filters and present quantitative comparisons of convergence between regularized and preconditioned inversion. They conclude that within the first few iterations of the preconditioned CGNE scheme, the most important characteristics of the model are obtained; small details added in later iterations do not alter the model much. The CGNE scheme usually can be stopped after these first few iterations. This means the term $\sigma_n^2\mathbf{I}$ in equation 13 can be ignored because limiting the number of CGNE iterations (within the IRLS iterations) acts as regularization of the inversion. This finding is supported by Trad et al. (2003) and Liu and Sacchi (2004), and numerous examples performed for this research.

The algorithm we use is listed in Table 1. It requires a matrix $\mathbf{H}$, which equals the Toeplitz matrix multiplied on both sides by the prior matrix $\mathbf{C}_{\tilde{p}i}^{1/2}$. The matrix $\mathbf{C}_{\tilde{p}i}$ destroys the Toeplitz structure; therefore, it is more efficient to evaluate multiplications with $\mathbf{H}$ in steps. Multiplication by the Toeplitz matrix is performed with fast Fourier transforms (FFTs), whereas multiplication by $\mathbf{C}_{\tilde{p}i}^{1/2}$ requires only an element-wise multiplication between vectors because it is a diagonal matrix. The IRLS iterations are started with the initial model equal to zero and the model weight matrix $\mathbf{C}_{\tilde{p}}$ computed from the NDFT estimate $\mathbf{A}^H\mathbf{W}\mathbf{p}$. Each time CGNE inversion converges, the next IRLS iteration starts. The model found by CGNE in the ith IRLS iteration is used as the starting model in the CGNE algorithm in the IRLS iteration $i + 1$ and is used to compute the matrix $\mathbf{C}_{\tilde{p}_{i+1}}$. Although convergence criteria can be designed for IRLS (see, for instance, Trad et al., 2003) we typically use a maximum of two to five IRLS iterations.

DOUBLE FRSI FOR INTERPOLATING NONUNIFORMLY SAMPLED ALIASED DATA

FRSI cannot handle aliased data, and Gulunay's method cannot handle nonuniformly sampled data. Here, we present a hybrid method based on FRSI and inspired by Gulunay's approach; it can handle nonuniformly sampled, aliased data.

First, we introduce the following parameters:

- L, the interpolation factor, indicates that for uniformly sampled, aliased data, $L - 1$ traces must be inserted between adjacent traces to remove the aliasing.
- f_{alias}, the frequency at which wraparound first occurs
- $f_{\max} = L \times f_{\text{alias}}$, the maximum frequency that can be corrected for aliasing
- $k_N = 1/(2\Delta x)$, the Nyquist wavenumber corresponding to sampling interval Δx of the coarsely sampled input data. The interpolated data have a sampling interval $\Delta x/L$ and a Nyquist wavenumber Lk_N.

Table 1. The algorithm for IRLS with CGNE used to invert the Fourier coefficients.

$i = 0$
$\tilde{\mathbf{p}}_i = \mathbf{0}$
Calculate $\mathbf{C}_{\tilde{p}_i}$ from $\mathbf{A}^H\mathbf{W}\mathbf{p}$ using equation 8
IRLS: while $i \le i_{\max}$
$k = 0$
$\mathbf{z}_k = \tilde{\mathbf{p}}_i$
$\mathbf{H} = \mathbf{C}_{\tilde{p}_i}^{1/2}\mathbf{A}^H\mathbf{W}\mathbf{A}\mathbf{C}_{\tilde{p}_i}^{1/2}$
$\mathbf{r}_k = \mathbf{C}_{\tilde{p}_i}^{1/2}\mathbf{A}^H\mathbf{W}\mathbf{p} - \mathbf{H}\mathbf{z}_k$
$\mathbf{d}_k = \mathbf{r}_k$
CGNE: while $\frac{\|\mathbf{r}_k\|}{\|\mathbf{r}_0\|} >$ limit, $k \le k_{\max}$
$\alpha = \frac{\|\mathbf{r}_k\|}{\mathbf{d}_k^H\mathbf{H}\mathbf{d}_k}$
$\mathbf{z}_{k+1} = \mathbf{z}_i + \alpha\mathbf{d}_k$
$\mathbf{r}_{k+1} = \mathbf{r}_i - \alpha\mathbf{H}\mathbf{d}_k$
$\beta = \frac{\|\mathbf{r}_{k+1}\|}{\|\mathbf{r}_k\|}$
$\mathbf{d}_{k+1} = -\mathbf{r}_{k+1} + \beta\mathbf{d}_k$
$k = k + 1$
$\tilde{\mathbf{p}}_{i+1} = \mathbf{C}_{\tilde{p}_i}^{1/2}\mathbf{z}_k$
Calculate $\mathbf{C}_{\tilde{p}_{i+1}}$ from $\tilde{\mathbf{p}}_{i+1}$
$i = i + 1$

Gulunay's *f-k* interpolation beyond aliasing

Interpolation of uniformly sampled, nonaliased data can be performed in the *f-k* domain by zero padding beyond the Nyquist wavenumber (k_N). When the data are aliased, replications of the nonaliased spectrum occur periodically along the wavenumber axis and fold into the desired wavenumber range, causing artifacts in the interpolated data. Gulunay's *f-k* interpolation for uniformly sampled, aliased data derives a mask to mute out these replications and leave only the nonaliased part of the spectrum.

When the data are spatially undersampled by a factor L, $L-1$ traces need to be interpolated between existing traces to remove the aliasing and to create a properly sampled data set. When, instead, $L-1$ zero traces are inserted between existing traces, the Nyquist wavenumber is increased to Lk_N, but now the spectrum in the range $[-Lk_N, Lk_N]$ contains the original spectrum as well as $L-1$ aliases of it because of the aliasing.

Gulunay uses the nonaliased part of the spectrum between wavenumbers $[-k_N, k_N]$ and temporal frequencies $[0, f_{\max}/L]$ to design a mask that is applied to the aliased spectrum obtained by inserting zero traces. To perform this element-wise multiplication, the nonaliased spectrum is interpolated such that it contains L times as many samples in each direction. This can be done by zero padding up to Lk_N and $f_{\max}$ and performing an inverse FFT to the spatial domain followed by an FFT back to the wavenumber domain. The mask filters out the aliases in the spectrum between wavenumbers $[-Lk_N, Lk_N]$ and temporal frequencies $[0, f_{\max}]$.

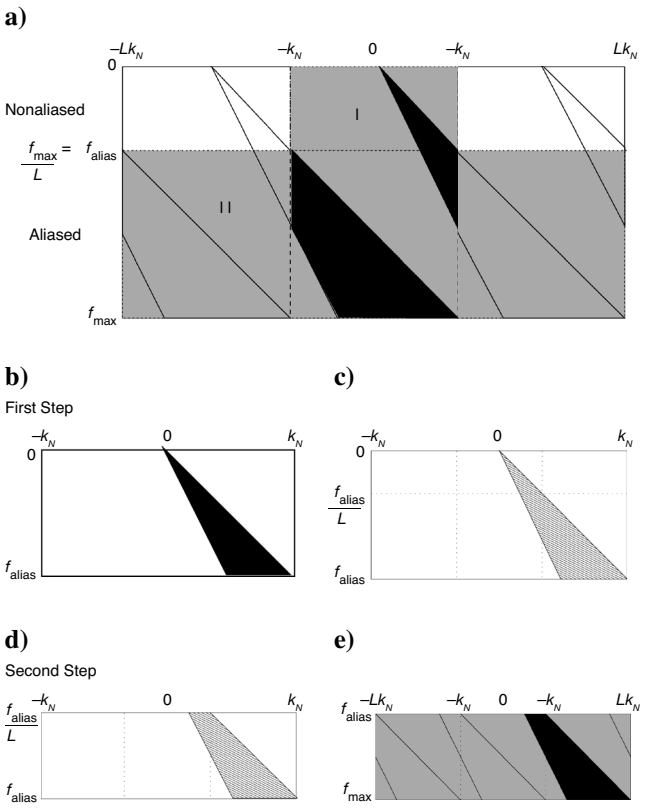

Figure 3. Schematic explanation of the double FRSI algorithm for $L = 3$. (a) Division of spectrum in two parts. (b) Step 1: Estimation of nonaliased spectrum. (c) The estimated spectrum is interpolated to the size of the spectrum that will be estimated in the second step. (d) Step 2: The prior $\mathbf{C}_{\tilde{p}}$ for the inversion in step 2. (e) The prior suppresses all coefficients except those in black, which represent nonaliased energy.

Double FRSI method

In the double FRSI method, FRSI is applied twice so that the coefficients estimated in the first pass can be used to separate the aliased from the nonaliased frequencies in the second pass. The spectrum is divided in two parts, as in Figure 3a. The difference between step one and step two is in the range of Fourier coefficients estimated and the prior matrix $\mathbf{C}_{\tilde{p}}$. In the first step the inversion is performed for the nonaliased Fourier coefficients in the wavenumber range $[-k_N, k_N]$, and for frequencies $[0, f_{\text{alias}}]$ (shown in black in Figure 3b), where f_{alias} is the frequency where the wrap-around first occurs. In the first step the prior $\mathbf{C}_{\tilde{p}}$ for sparse inversion is calculated from the NDFT coefficients using equation 9, the model weighting function.

In the second pass, the inversion is performed for the frequency range $[0, f_{\max}]$ and wavenumber range $[-Lk_N, Lk_N]$. The spectrum estimated in the first pass is interpolated and stored in a matrix $\mathbf{D}$. The interpolation is performed such that $\mathbf{D}$ has the same dimensions as the spectrum estimated in the second pass, as indicated in Figure 3c. The interpolation is performed by zero padding the nonaliased spectrum between k_N and Lk_N and performing an inverse FFT to the spatial domain followed by an FFT back to the wavenumber domain. For each frequency f, in the second pass, the row with index $f/\Delta f$ from $\mathbf{D}$ is used to construct the prior $\mathbf{C}_{\tilde{p}}$ for sparse inversion using equation 9, the model weighting function. The matrix $\mathbf{D}$, shown in Figure 3d, is used to distinguish aliased energy from the nonaliased spectrum, in Figure 3e, and acts as a parameter selection tool. For a data set consisting of planar events, $\mathbf{C}_{\tilde{p}}$ will suppress the aliases. When aliased energy wraps around in the range of nonaliased energy, the method will still work. The method is designed to distinguish between aliased and nonaliased energy. When aliased overlies nonaliased energy, then remnants of aliased energy for that particular wavenumber/frequency can be expected in the data.

To automatically detect where the aliasing starts in the case of regular sampling, one can think of monitoring the result of FRSI in the first pass to detect the temporal frequency at which the spatial Fourier coefficients near the Nyquist wavenumber become comparable in magnitude to those of the desired signal; the desired signal can be defined as the spatial Fourier coefficients within a wedge/cone defined by a minimum apparent velocity. For nonuniform sampling, the phenomenon of aliasing becomes more diffuse; hence, it becomes more difficult to quantify and discriminate from sampling artifacts.

The idea to use coefficients obtained at low frequencies to construct a model weighting matrix for the inversion at higher frequencies is also used by Herrmann et al. (2000) for the high-resolution Radon transform. Their method uses the coefficients obtained at the previous frequency to construct the model weighting matrix for the current frequency. This works for the Radon transform, where one planar or parabolic event maps to the same location on the slope/curvature axis in the Radon domain for all temporal frequencies.

EXAMPLES IN ONE SPATIAL DIMENSION

Aliased planar events: Uniform sampling with gaps

Figure 4 shows results of the double FRSI algorithm on four uniformly sampled planar events, but with missing traces. For the examples with planar events, all data were used at once, i.e., no spa-

tiotemporal windows were used. We did constrain the spatial bandwidth in the inversion with a symmetric, frequency-dependent spatial bandwidth, determined by the maximum dip in the data. The double FRSI algorithm works very well on aliased, planar events with only positive or only negative dips that do not overlap in the Fourier domain. A more difficult example is given in Figure 5a, which shows a data set with eight planar events dipping in opposite directions. Every other trace from the original 132 traces has been omitted and an additional 11 traces have been killed. The result is aliasing by a factor $L = 2$ and artifacts in the spectrum because of the additional gaps (Figure 5b). The double FRSI reconstruction is shown in Figure 5c. We use equation 9, the model weighting function, with $a = 2$ and set $\sigma_{\tilde{p}}^2$ as 10% of the maximum of the squared NDFT coefficients. As discussed previously, the limited number of iterations in the CGNE algorithm stabilizes the inversion; therefore, σ_n^2 can be ignored. We also constrain the bandwidth with a minimum apparent velocity cone of ± 120 m/s. We perform the inversion with the (smoothed) model preconditioned conjugate gradient algorithm using two IRLS iterations. The larger the value of $\sigma_{\tilde{p}}^2$, the larger the remaining aliased energy. On the other hand, the smaller the value of $\sigma_{\tilde{p}}^2$, the more the desired signal is suppressed. Therefore, $\sigma_{\tilde{p}}^2$ must be chosen with some care. An alternative way to set the model sparseness is by varying the sparseness function through parameter a in the model weighting function (equation 9).

The difference between the reconstruction and the original noise free data is shown in Figure 5e (amplitude $\times 4$). Figure 5d shows that aliased energy which does not interfere with the desired spectrum has been removed, but the estimation is suboptimal for frequencies where aliased energy overlaps nonaliased energy. This is because the prior $\mathbf{C}_{\tilde{p}}$ used in the inversion of the second pass acts only as a parameter-selection mechanism and cannot separate aliased and nonaliased energy where they overlap. The prior $\mathbf{C}_{\tilde{p}}$ itself is shown in Figure 5f.

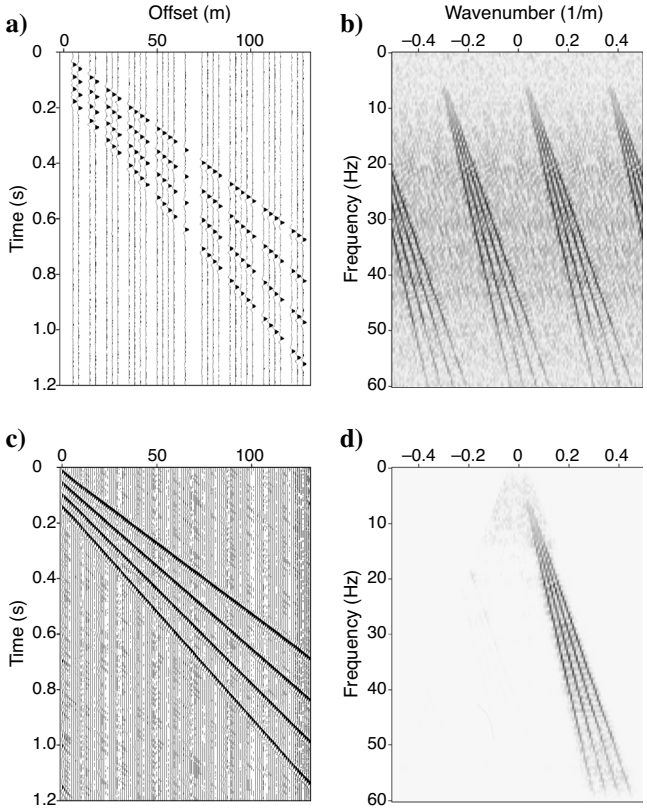

Figure 4. (a) Noisy, aliased data with missing traces. (b) Its amplitude spectrum. (c) Reconstruction with double FRSI algorithm. (d) Estimated Fourier coefficients.

Aliased marine shot record: Uniform sampling

Figure 6a shows an aliased marine shot record consisting of 45 traces. Because two out of three traces are missing ($L = 3$), the two ($L - 1$) aliases are clearly visible in the amplitude spectrum in Figure 6c. We applied the double FRSI algorithm in overlapping spa-

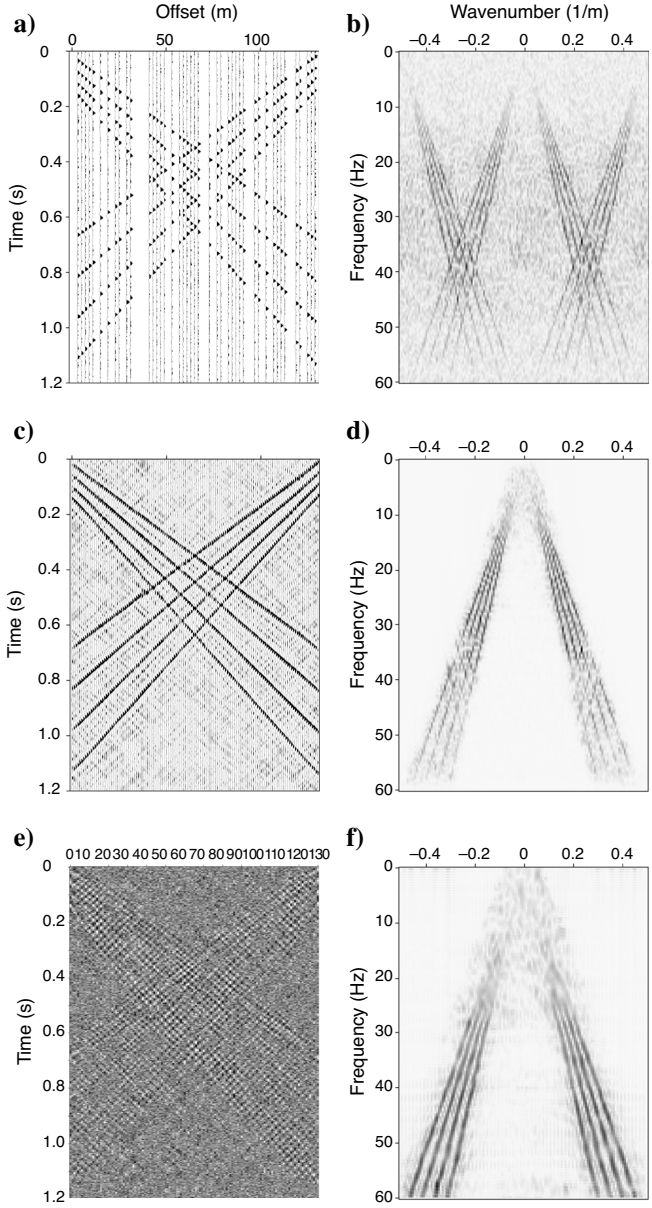

Figure 5. (a) Noisy, aliased data with missing traces and (b) its amplitude spectrum. (c) Reconstruction with double FRSI algorithm and (d) estimated Fourier coefficients. (e) Difference between reconstruction and correct data (amplitude $\times$ 4). (f) Prior $\mathbf{C}_{\tilde{p}}$ used to suppress aliasing in the second pass.

tiotemporal windows, in which the assumption of planar events approximately holds. The size of the overlapping windows was 64 time samples with 16 samples overlap and 10 traces (375 m) with five traces overlap. To further reduce aliasing, we constrained the spatial bandwidth in the inversion by a velocity cone of $c_{\min} = \pm 1500$ m/s ($k_{\max} = f/c_{\min}$). Although application of NMO is beneficial because it reduces the spatial bandwidth by flattening the hyperbolic events, it was not applied in this example to make the example a little more difficult. We added some noise before the first break to stabilize the inversion, which was removed by a first-break mute after reconstruction. We used $a = 2$ in equation 9, the model weighting function, and set $\sigma_{\bar{p}}^2$ as 1% of the maximum of the squared NDFT coefficients. We used the model preconditioned CGNE algorithm with two IRLS iterations. Figure 6b shows the reconstruction, and Figure 6d shows the amplitude spectrum of the reconstructed data. Figure 7a shows the difference between the original and interpolated data, with amplitude multiplied by a factor of four.

Aliased marine shot record: Uniform sampling with gaps

In the previous example, the sampling is completely uniform; therefore, Fourier reconstruction reduces to a band-limited sinc interpolation because $\mathbf{A}^H \mathbf{A} = \mathbf{I}$ in equation 8. In this case, the double FRSI algorithm becomes almost equivalent to Gulunay's algorithm. A more interesting problem (in the context of this article, at least) is the reconstruction of aliased seismic data in case of uniform sampling with gaps. Figure 8 shows the same aliased marine shot record

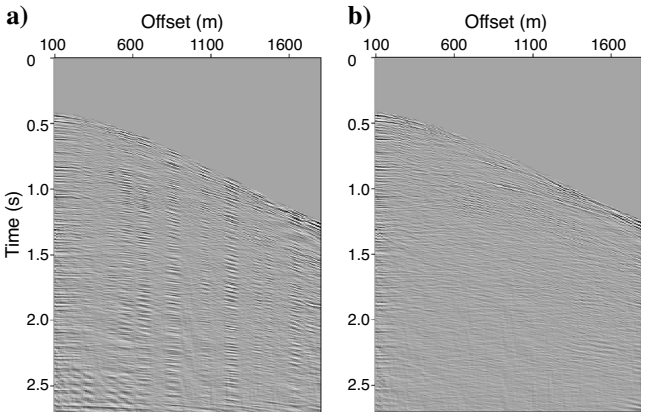

Figure 7. Difference plot for reconstruction in (a) Figure 6b and (b) Figure 8b. The amplitude in both difference plots is multiplied by a factor of four.

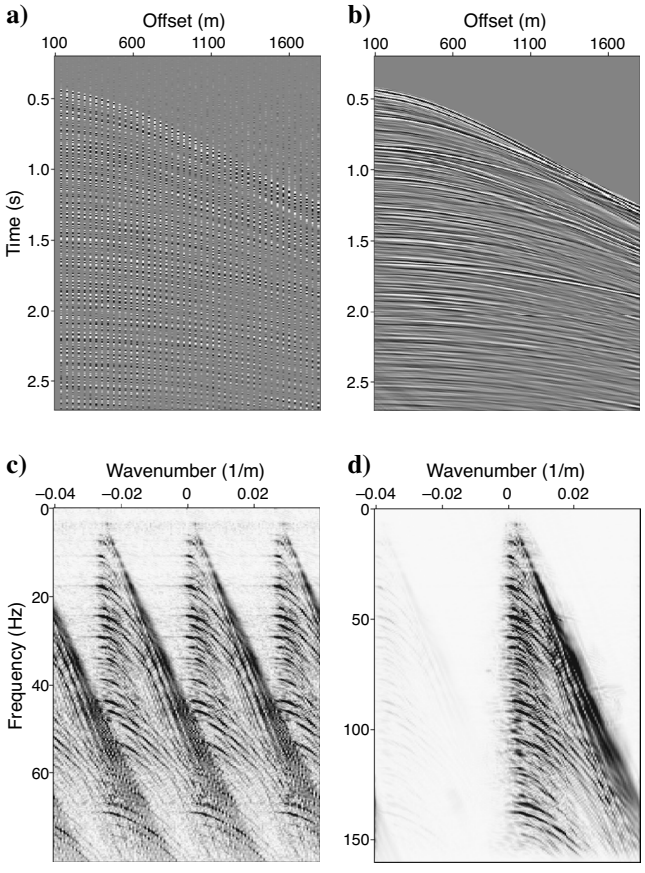

Figure 6. (a) Uniformly sampled, aliased marine shot record (Δx = 37.5 m) and (c) its amplitude spectrum. (b) Result of two-pass FRSI reconstruction and (d) corresponding amplitude spectrum with the aliases removed.

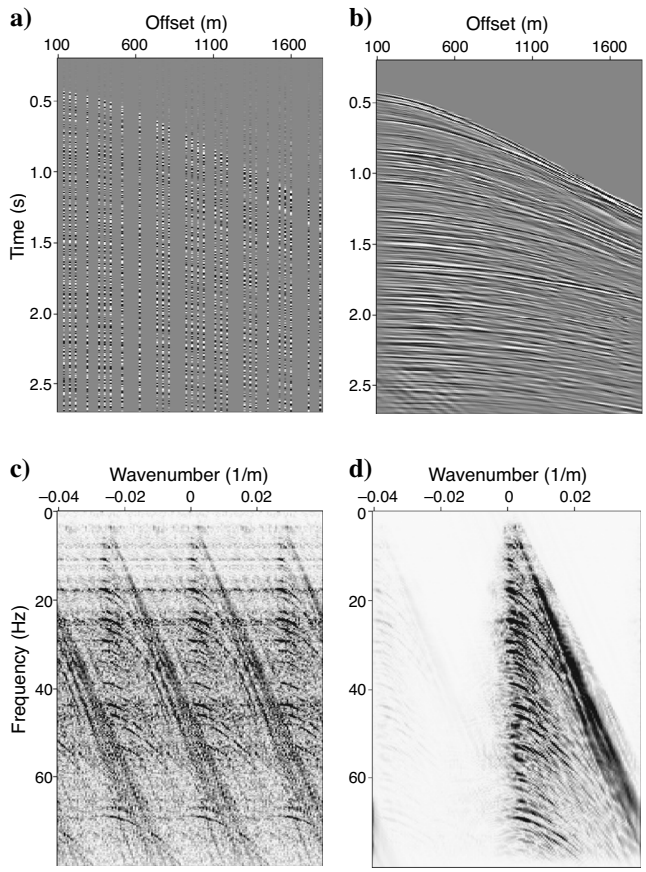

Figure 8. (a) Shot gather of Figure 6a with an additional randomly selected 17 traces removed and (c) its amplitude spectrum. (b) Result of double FRSI reconstruction applied in overlapping windows and (d) the estimated amplitude spectrum.

as in Figure 6, only an additional randomly selected 17 traces have been removed, resulting in a maximum gap size of eight traces. Figure 8c shows aliasing and the sampling related distortions of the spectrum. The parameters for the double FRSI algorithm are the same as in the previous example, except for the spatial window size, which contained all traces within a 600-m sliding window with half a window size overlap. Again, we did not use NMO to reduce the bandwidth. The double FRSI has removed the aliasing and distortion in the spectrum quite well, as seen in Figure 8b and d. Figure 7b shows the difference between the original and interpolated data, with amplitude multiplied by a factor of four. The difference plot shows that the interpolation result is good but that at the positions of the larger gaps the interpolation error is higher, as could be expected.

EXAMPLES IN TWO SPATIAL DIMENSIONS

Extension of Gulunay's method and Fourier reconstruction to higher dimensions is straightforward and is explained in detail in Gulunay (2003) and Hindriks and Duijndam (2000). We refer the reader to these two articles for implementation aspects. The 2D double FRSI algorithm is analogous to the 1D case. But if the inversion in the first pass is performed for M Fourier coefficients, the inversion in the second pass will require $L^D M$ parameters, where D is the dimension of the problem. This parameter increase does not pose problems for the double FRSI algorithm in two spatial dimensions, but in three spatial dimensions it becomes an issue for both the handling of the aliasing as well as the efficiency of the method.

Aliased planar events: Uniform sampling with and without random perturbations

Figure 9a–c shows three 2D sampling geometries, one of which is completely uniform and two that are uniform with a random deviation in the coordinates of maximum 25% and 50% of the sampling interval. There are 196 traces (14×14) with a sampling interval of $\Delta x = \Delta y = 3$, and the data are undersampled by a factor $L = 3$. In the first pass of FRSI, we estimate the nonaliased part of the spectrum below 20 Hz for all the data at once (no windowing). At each frequency, an inversion is performed for 15×15 Fourier coefficients (7 positive + 7 negative + 0) in the 2D wavenumber plane. In the second pass, the inversion is performed up to 60 Hz for a wavenumber plane consisting of 43×43 Fourier coefficients (21 positive + 21 negative + 0), which means there are nine times as many parameter as input data. The reconstruction results for the standard FRSI algorithm are shown in Figure 10a–c, with corresponding spectra in Figure 10d–f. The results of the double FRSI algorithm are shown in Figure 10g–i, with corresponding spectra in Figure 10j–l. For the prior $\mathbf{C}_{\bar{p}}$, we used equation 9, the model weighting function, with $a = 2$ and set $\sigma_{\bar{p}}^2$ as 1% of the maximum of the squared NDFT coefficients. The reconstruction with the standard FRSI algorithm took 18 s, whereas the double FRSI algorithm took 25 s on one SGI Origin 200 CPU to invert 122 frequency slices.

As the sampling irregularity increases, the aliases become less pronounced. Because of this, the standard FRSI reconstruction result improves with increasingly less uniform sampling (Figure 10d–f). The double FRSI algorithm correctly reconstructs the data for all geometries.

Synthetic 2D seismic survey: Uniform sampling with gaps

The geologic model for the synthetic data in this example is a tilted fault-block model, overlain by several horizontal reflectors and simulating the situation in some parts of the North Sea. Wever and Spetzler (2004) use this 2D synthetic data in a time-lapse experiment to test the sensitivity of several time-lapse metrics to acquisition per-

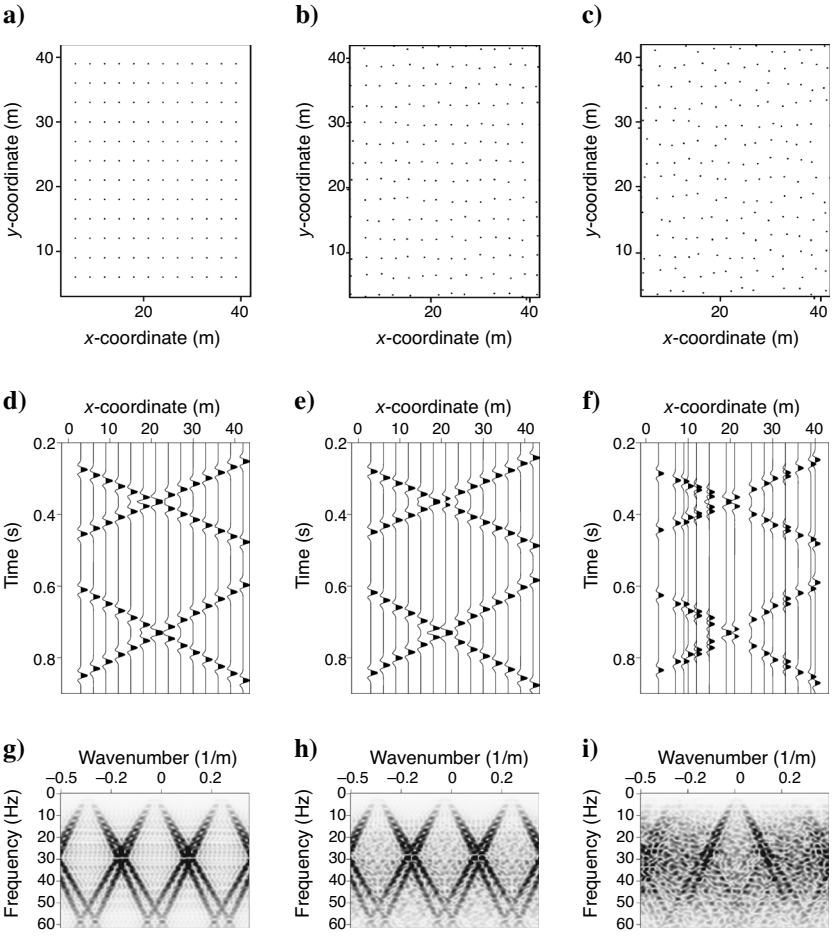

Figure 9. (a) Cartesian sampling with 196 traces and $\Delta x = \Delta y = 3$, and sampling geometries with a maximum random error in sampling of (b) $0.25\Delta x$ and (c) $0.5\Delta x$. (d) Gather from (a) with $y = 20$ and (g) its amplitude spectrum. (e) and (f) Gather from (b) and (c), respectively, with y between $[19.5, 20.5]$ and (h) and (i) their amplitude spectra.

turbations and to show how 1D Fourier reconstruction can benefit time-lapse processing. Here, we use it for a reconstruction experiment in two spatial dimensions. The data set was generated through finite-difference modeling, simulating a split-spread configuration. The shot spacing was 25 m and receiver spacing was 24 m. Figure 11a shows the input data after additionally randomly removing 20% of the remaining traces to introduce irregularity in the sampling. We performed the reconstruction in the 2D shot-offset domain, but the method can also be applied in the shot-receiver or midpoint-offset domains.

The double FRSI algorithm was applied in overlapping spatiotemporal windows that were 80 ms long with 20-ms overlap. In the spatial directions, we used 20 shots simultaneously and all traces within an offset window of approximately 300 m in length, corresponding to approximately 12 traces. The overlap in offset direction was 150 m. We used an interpolation factor $L = 2$ and a maximum frequency of 60 Hz. In the previous examples, the planar events were all of approximately equal strength, but this example contains both strong and weak reflections. A value of $a = 2$ for $\mathbf{C}_{\bar{p}}$ in the model weighting function (equation 9) attenuated the weaker events too much, but $a = 1$ gave good results. We set the tuning parameter $\sigma_{\bar{p}}^2$ again as 1% of the squared NDFT coefficients. The output shot and offset intervals were both set to 12.5 m (Figure 12b). A gather from the reconstructed data (Figure 12a) shows aliasing has been removed from the flanks of the hyperbolas. The f-k spectrum in Figure 12b also shows this gather is not aliased.

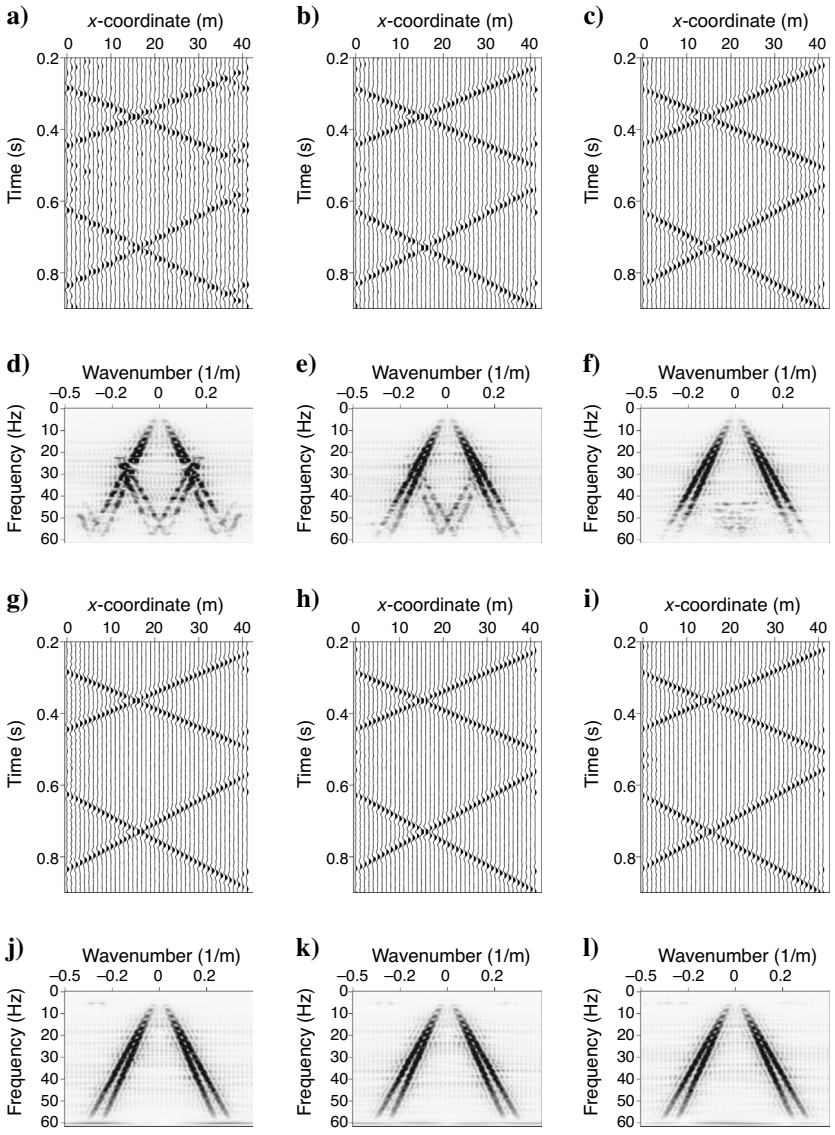

Figure 10. Reconstruction of data in the corresponding columns in Figure 9. (a–f) Standard FRSI. (g–l) Double FRSI.

Cascade of FRSI and Gulunay's method

An alternative algorithm to the double FRSI method is to use a cascade of FRSI (Zwartjes and Duijndam, 2000) and Gulunay's f-k interpolation method (Gulunay, 2003), an idea suggested by Abma and Kabir (2003) under the name *nonaliased FK method*. We have applied such a cascaded method successfully to uniformly sampled data with and without samples missing (results not shown). However, a problem with this method is that as the sampling deviates from fully uniform with missing samples to sampling with positioning errors and missing samples, the aliasing becomes more diffuse until it disappears in the sampling artifacts for random sampling. The diffused nature of the aliased energy makes it difficult for Fourier reconstruction to produce an aliased spectrum without sampling distortions. Gulunay's algorithm will not remove this dispersed aliased energy. Therefore, as sampling becomes less uniform, the cascaded approach becomes less successful. In the extreme case of random sampling, this is no longer an issue because of the absence of aliasing. An advantage of the cascaded algorithm is that in higher dimensions it does not suffer from the strong increase of parameters as the double FRSI method does.

DISCUSSION

The underlying assumption for the interpolation beyond aliasing with the double FRSI method is that the data consist of a limited number of planar events. When the data do not consist of planar events, the method can be applied in overlapping spatiotemporal windows. Window sizes are generally on the order of 100 ms and 10–15 traces in each spatial dimension. Because the spatial bandwidth of the data increases with offset, the application of time/space-variant sparseness constraint may be beneficial when working with overlapping windows, although we have not verified this. When no window can be designed in which the data consist of planar events, a transform with basis functions that better describe the move-out of the data will be more suitable. A good example of this is the application of the

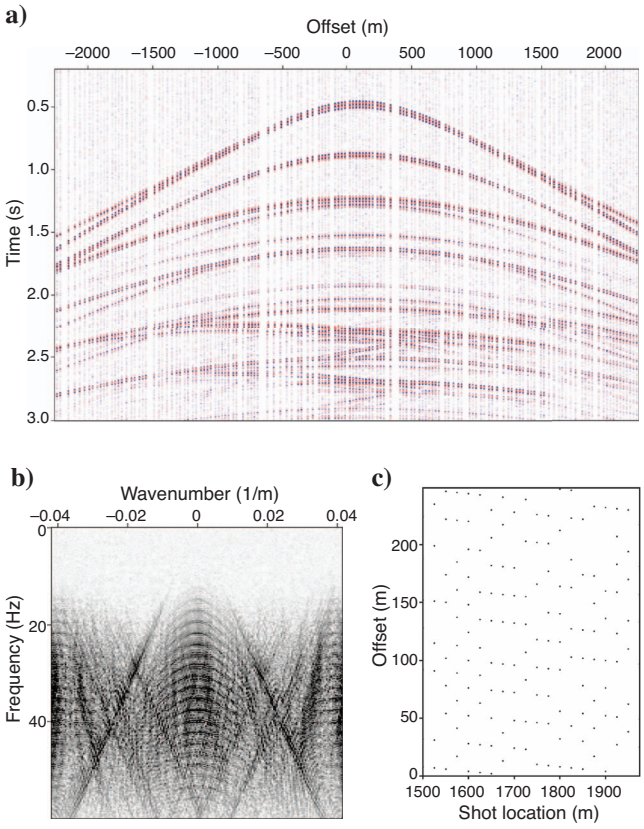

Figure 11. Synthetic data two times undersampled and a randomly selected 20% of the remaining data removed. (a) Shot record from the synthetic survey and (b) its amplitude spectrum. (c) Sampling geometry of part of the survey, shot versus offset.

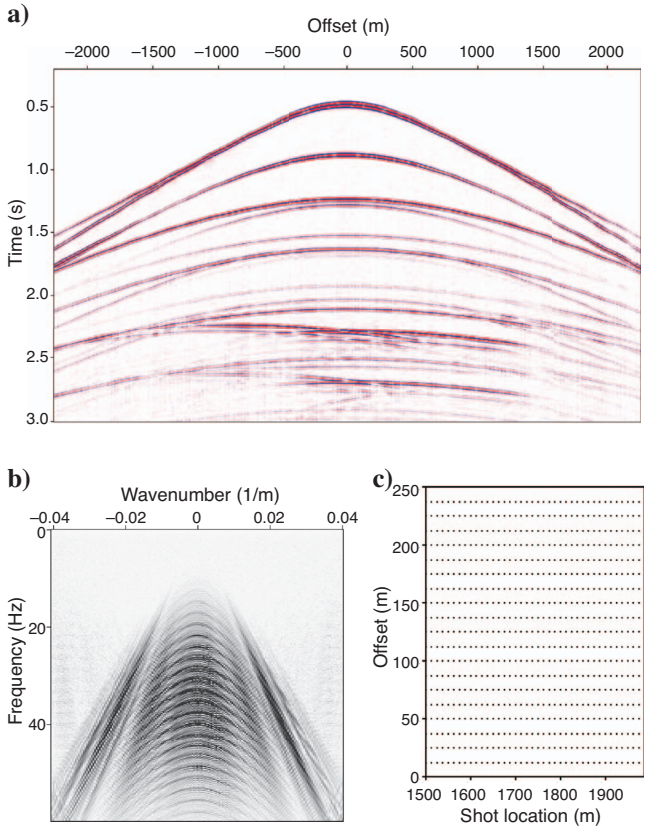

Figure 12. Synthetic data two times undersampled and a randomly selected 20% of the remaining data removed. (a) Shot record from the reconstructed survey and (b) its amplitude spectrum. (c) Sampling geometry after reconstruction, shot versus offset.

high-resolution parabolic and hyperbolic Radon transforms (Herrmann et al. 2000; van Dedem and Verschuur, 2000).

To suppress aliased energy adequately, the tuning parameters for the model weighting matrix must be set properly. Choosing too much sparseness may suppress weak energy; so in general, it is a good idea to apply some form of gain to equalize amplitudes in the data before reconstruction. The method has the following limitations. First, the maximum temporal frequency that can be corrected for aliasing depends on the highest nonaliased temporal frequency. As the aliasing becomes more severe, the nonaliased region shrinks. There is, therefore, a limit to how much aliasing can be handled. Second, the algorithm only discriminates between aliased and nonaliased coefficients and cannot discriminate between aliased and nonaliased energy for a single coefficient. For this reason overlapping of aliased and nonaliased energy still presents a challenge. Third, small spatiotemporal windows are used to reconstruct nonplanar events. When gap sizes are of the same order as the windows required to obtain approximately planar events, the method will obviously be less effective. In general, the reconstruction error increases with gap size. Finally, if in the first step of the double FRSI algorithm the number of parameters estimated is M, then in the second step there are ML^D parameters, where L is the interpolation factor and D the number of spatial dimensions. For $L \leq 4$ and $D \leq 2$, good results have been obtained in synthetic and real data tests. For $D \geq 3$, the number of parameters increases dramatically with respect to the available input data. However, when applied to multidimensional aliased data, the algorithm assumes aliasing along each spatial dimension. In practice, this need not always be the case, and this may be exploited by extending the wavenumber axis only along the aliased direction.

CONCLUSION

The double FRSI algorithm combines the principles of Fourier reconstruction with sparse inversion, which cannot handle aliasing, and the *f-k* interpolation algorithm, which cannot handle nonuniform sampling, into a new method that can reconstruct nonuniformly sampled aliased seismic data. As with many existing methods, we assume the data consist of a limited number of planar events. Therefore, the algorithm should be applied to seismic data in overlapping spatiotemporal windows.

The use of the nonaliased part of the spectrum to help dealias the data is inspired by Gulaney's *f-k* interpolation method for uniformly sampled, aliased data. How the prior is obtained from the nonaliased part of the spectrum is similar to how the mask is obtained in Gulunay's method. However, in the double FRSI algorithm, the prior is both estimated and applied in a least-squares manner, while Gulunay's mask is estimated and applied as an element-wise division and multiplication only. This makes the double FRSI method able to handle nonuniform sampling.

The method shows good results in the reconstruction of nonuniformly sampled, aliased seismic data in one and two spatial dimensions. An interesting aspect is that as the sampling becomes less uni-

form and approaches a more random sampling scheme, the effect of aliasing disappears, leaving only artifacts in the Fourier domain from the nonuniform sampling, which can be removed with the standard Fourier reconstruction algorithm.

ACKNOWLEDGMENTS

The authors thank Dries Gisolf and Eric Verschuur (Delft University of Technology) for constructive discussions about this research. All sponsors of DELPHI's Acquisition and Preprocessing project are gratefully thanked for their financial support. The reviewers are thanked for their feedback that helped improve this paper.

REFERENCES

Abma, R., and N. Kabir, 2003, Comparisons of interpolation methods in the presence of aliased events: 73rd Annual International Meeting, SEG, Expanded Abstracts, 1909–1912.

Bardan, V., 1987, Trace interpolation in seismic data-processing: Geophysical Prospecting, **38**, 343–358.

Claerbout, J., and S. Fomel, Image estimation by example: ⟨http://sepwww-.stanford.edu/⟩.

Claerbout, J., and F. Muir, 1973, Robust modeling with erratic data: Geophysics, **38**, 826–844.

Claerbout, J. F., and D. Nichols, 1991, Interpolation beyond aliasing by (tau,x)-domain PEFs: 53rd Annual Conference and Exhibition, EAGE, Extended Abstracts, 2–3.

Clippard, J. D., D. H. Christensen, and R. D. Rechtien, 1995, Composite distribution inversion applied to crosshole tomography: Geophysics, **60**, 1283–1294.

Crawley, S. J. C., and R. Clapp, 1999, Interpolation with smoothly nonstationary prediction-error filters: 69th Annual International Meeting, SEG, Expanded Abstracts, 1154–1157.

Duijndam, A. J. W., and M. A. Schonewille, 1999, Nonuniform fast Fourier transform: Geophysics, **64**, 539–551.

Duijndam, A. J. W., M. A. Schonewille, and C. O. H. Hindriks, 1999, Reconstruction of band-limited signals, irregularly sampled along one spatial direction: Geophysics, **64**, 524–538.

Feichtinger, H., K. Gröchenig, and T. Strohmer, 1995, Efficient numerical methods in nonuniform sampling theory: Numerische Mathematik, **69**, 423–440.

Fomel, S., 2002, Applications of plane-wave destruction filters: Geophysics, **67**, 1946–1960.

Gulunay, N., 2003, Seismic trace interpolation in the Fourier transform domain: Geophysics, **68**, 355–369.

Hansen, P., 1998, Rank-deficient and discrete ill-posed problems: Numerical aspects of linear inversion: Society of Industrial and Applied Mathematics.

Herrmann, P., T. Mojesky, M. Magesan, and P. Hugonnet, 2000, De-aliased, high-resolution Radon transforms: 70th Annual International Meeting, SEG, Expanded Abstracts, 1953–1956.

Hindriks, K., and A. Duijndam, 2000, Reconstruction of 3D seismic signals irregularly sampled along two spatial coordinates: Geophysics, **65**, 253–263.

Högbom, J. A., 1974, Aperture synthesis with a non-regular distribution of interferometric baselines: Astronomy and Astrophysics Supplement Series, **15**, 417–426.

Kao, C., 1997, A trace interpolation method for spatially aliased and irregularly spaced seismic data: 71st Annual International Meeting, SEG, Expanded Abstracts, 1108–1110.

Liu, B., 2004, Multi-dimensional reconstruction of seismic data: Ph.D. dissertation, University of Alberta.

Liu, B., and M. Sacchi, 2001, Minimum weighted norm interpolation of seismic data with adaptive weights: 71st Annual International Meeting, SEG, Expanded Abstracts, 1921–1924.

———, 2004, Minimum weighted norm interpolation of seismic records: Geophysics, **69**, 1560–1568.

Liu, B., M. Sacchi, and H. Kuehl, 2003, 2D/3D seismic wavefield reconstruction for AVA imaging: 73rd Annual International Meeting, SEG, Expanded Abstracts, 235–238.

Pipe, J. G., and P. Menon, 1999, Sampling density compensation in MRI: Rationale and an iterative numerical solution: Magnetic Resonance in Medicine, **41**, 179–186.

Sacchi, M. D., and T. J. Ulrych, 1995, High-resolution velocity gathers and offset space reconstruction: Geophysics, **60**, 1169–1177.

———, 1996, Estimation of the discrete Fourier transform: A linear inversion approach: Geophysics, **61**, 1128–1136.

Soubaras, R., 1997, Spatial interpolation of aliased seismic data: 67th Annual International Meeting, SEG, Expanded Abstracts, 1167–1170.

Spitz, S., 1991, Seismic trace interpolation in the F-X domain: Geophysics, **56**, 785–794.

Thorson, J. R., and J. F. Claerbout, 1985, Velocity stack and slant stochastic inversion: Geophysics, **50**, 2727–2741.

Trad, D., T. Ulrych, and M. Sacchi, 2003, Latest views of the sparse Radon transform: Geophysics, **68**, 386–399.

van Dedem, E. J., and D. J. Verschuur, 2000, 3D surface-related multiple prediction, an inversion approach: 70th Annual International Meeting, SEG, Expanded Abstracts, 1965–1968.

Wajer, F. T. A. W., G. H. L. A. Stijnman, M. Fuderer, A. F. Mehlkopf, D. Graverond-Demilly, and D. van Ormondt, 1998, MRI measurement time reduction by undersampling and Bayesian reconstruction using a 2D Lorentzian prior: Proceedings of the 4th Annual Conference, Advanced School for Computing and Imaging, 147–153.

Wever, A., and J. Spetzler, 2004, Criteria for source and receiver positioning in time-lapse seismic acquisition: 74th Annual International Meeting, SEG, Expanded Abstracts, 2319–2322.

Xu, S., Y. Zhang, D. Pham, and G. Lambare, 2005, Antileakage Fourier transform for seismic data regularization: Geophysics, **70**, no. 4, V87–V95.

Zhang, Z. Y., 1997, Parameter estimation techniques: A tutorial with respect to conic fitting: Image and Vision Computing, **15**, no. 1, 59–76.

Zwartjes, P. M., and A. J. W. Duijndam, 2000, Optimizing reconstruction for sparse spatial sampling: 70th Annual International Meeting, SEG, Expanded Abstracts, 2162–2165.

Zwartjes, P., and C. Hindriks, 2001, Regularising 3D data using Fourier reconstruction and sparse inversion: 63rd Annual Conference and Exhibition, EAGE, Extended Abstracts, Session A-15.